IRMPD Spectroscopic and Theoretical Structural Investigations of Zinc and Cadmium Dications Bound to Histidine Dimers

Brandon C. Stevenson, † Jonathan Martens, ‡ Giel Berden, ‡ Jos Oomen, $s^{\ddagger,\S}$ Mathias Schäfer, $^{\times}$ and P. B. Armentrout, *,†

[†]Department of Chemistry, University of Utah, 315 South 1400 East, Room 2020, Salt Lake City, Utah 84112, USA

[‡]Radboud University, Institute for Molecules and Materials, FELIX Laboratory, Toernooiveld 7, 6525 ED Nijmegen, The Netherlands

Abstract. Metallated gas-phase structures consisting of a deprotonated and an intact histidine (His) ligand, yielding M(His-H)(His)⁺ where M = Zn and Cd, were examined with infrared multiple photon dissociation (IRMPD) action spectroscopy utilizing light from a free-electron laser (FEL). In parallel, quantum chemical calculations identified several low-energy isomers for each complex. Experimental action spectra were compared to linear spectra calculated at the B3LYP level of theory, using the 6-311+G(d,p) and def2-TZVP basis sets for the zinc and cadmium complexes, respectively. For both the Zn and Cd species, definitive assignment is complicated by conflicting relative energetics, which were calculated at B3LYP, B3LYP-GD3BJ, B3P86, and MP2(full) levels. Spectral comparison for both species indicates that the dominant conformation, [N_{α},N_{π},CO⁻][CO₂⁻](N_{π}H⁺), has the deprotonated His chelating the metal at the amine nitrogen, π nitrogen of the imidazole ring, and the deprotonated carbonyl oxygen and the intact His ligand adopts a salt-bridge bidentate binding motif, coordinating the metal with both carboxylate oxygens. There is also evidence for a conformation where the deprotonated His coordination is maintained, but the intact His ligand adopts a more canonical structure, coordinating with the metal atom at the amine nitrogen and π nitrogen, [N_{α},N_{π},CO⁻][N_{α},N_{π}]gtgg. For both metallated species,

^{*} Department of Chemistry, University of Cologne, 50939 Cologne, Germany

[§]van't Hoff Institute for Molecular Sciences, University of Amsterdam, Science Park 904, 1098 XH Amsterdam, The Netherlands

^{*} Corresponding author, e-mail: armentrout@chem.utah.edu

B3LYP, B3P86, and B3LYP-GD3BJ levels of theory appear to describe the relative stability of the dominant zwitterionic species more accurately than the MP2(full) level.

Introduction

Zinc is found to play a significant role in both the structure and utility of proteins, where it acts to catalyze metabolic pathways, synthesize macromolecules, induce DNA repair, and stabilize protein folding. One class of zinc-containing macromolecules is the zinc finger proteins, where the classic binding motif has the zinc directly coordinated to two cysteine residues and two histidine (His) residues, as found in transcription factor IIIA. Estimates suggest that 1% of all mammalian genes encode zinc finger proteins, and these proteins play a role in mediating protein-protein interaction, protein folding, and cell-signaling. Zinc also promotes the aggregation of histidine-rich amyloid- β -peptides (A β), which are a major pathological event in Alzheimer's disease. This promotion is a result of zinc's favorable interaction with histidine, and the ability to cross-link the peptide through intermolecular His(N $_{\tau}$)-Zn²⁺-His(N $_{\tau}$) bridges. 6-8

One strategy to examine the interactions between metals and proteins is to simplify the complex being observed by chelating the metal ion to the relevant amino acids. This biomimetic complex, in the absence of solvent effects, can be interrogated to enhance our understanding of the more complicated biological systems. In the present work, the zinc dication was simultaneously complexed with a deprotonated histidine (His-H) and an intact histidine (His) ligand. The identity of the metal ion is an important consideration, and as such, the analogous cadmium complex, Cd(His-H)(His)⁺, was also investigated. Zinc and cadmium are closely related Group 12 metals that share valence electronic configurations and oxidation states (+2), and have similar ionic radii (Zn²⁺, 0.60 Å; Cd²⁺, 0.78 Å). Cadmium has been shown to replace zinc in zinc finger motifs, which inhibits the activity of the active metal site. Here, infrared multiple photon dissociation (IRMPD) action spectroscopy was used to examine the experimentally formed complexes of Zn(His-H)(His)⁺ and Cd(His-H)(His)⁺. These action spectra were then compared to calculated

spectra for low-energy conformers to determine the most populated conformations present and thus the binding character of these complexes. This investigation serves as an extension of earlier studies investigating zinc and cadmium cationized amino acids: histidine monomer and dimer (His),¹¹ cysteine (Cys) and cysteine methyl ester (Cys-OMe),¹² glutamine (Gln),¹³ serine (Ser),¹⁴ asparagine (Asn),¹⁵ glutamic acid (Glu),¹⁶ aspartic acid (Asp),¹⁷ arginine (Arg),¹⁸ lysine (Lys),¹⁹ threonine (Thr),²⁰ and methionine (Met).²¹

Experimental and Computational Section

Materials and Synthesis

Precursors to the Zn(His-H)(His)⁺ and Cd(His-H)(His)⁺ complexes were formed using a procedure adapted from the literature, and all materials were used as delivered and without further purification.²² Briefly, an aqueous solution (6 mL) of L-histidine (0.3 mmol) and pyridine (0.1mmol) was placed in a tube. Three mL of a metal salt solution (0.1 mmol), either zinc or cadmium acetate, in ethanol was carefully layered on top. The tube was allowed to stand at room temperature for approximately one week, resulting in the formation of a colorless, clear solution. This literature procedure suggests that crystal formation is enhanced by the slow diffusion of the reactants in this approach. Aliquots of a few μl of the stock solution were diluted with methanol to sub-millimolar concentrations for analysis.

Mass Spectrometry and Photodissociation

Infrared experiments were performed at the Free Electron Laser for Infrared eXperiments (FELIX) facility at Radboud University in Nijmegen, the Netherlands.²³ IRMPD spectroscopy was conducted using a quadrupole ion trap mass spectrometer (Bruker, Amazon Speed ETD), which had been modified to allow optical access to the ion trap for coupling to the free-electron laser (FEL).²⁴ The Zn(His-H)(His)⁺ and Cd(His-H)(His)⁺ ions were generated using an electrospray ionization (ESI) source from the prepared solutions. Trapped ions were then irradiated with light from the FELIX laser over an approximate 580 – 1800 cm⁻¹ spectral range, where the bandwidth

of the laser is 0.5% of the central frequency. The laser operated at a 10 Hz macropulse repetition rate with energy up to 114 mJ per pulse. Different laser attenuations were used, as indicated in the figures, in order to ensure that saturation did not obscure spectral features while still allowing weaker features to be observed. Unless otherwise noted, ions were irradiated with two macropulses.

IRMPD spectra were produced by plotting the yield as the natural logarithm of the photofragmentation yield, $Y = -\ln[\Sigma I_P /(\Sigma I_F + \Sigma I_P)]$, where I_F and I_P are the integrated intensities of the precursor and fragment ion mass peaks as a function of the FEL laser frequency.²⁵ For the Zn complex, precursor masses that were monitored included m/z 373, 374, 375, and 376, which includes most isotopes of Zn, ⁶⁴Zn (49.2%) along with contributions from ¹³C, ⁶⁶Zn (27.7%), and ⁶⁷Zn (4.0%). For the Cd complex, m/z 419, 420, 421, 422, and 423 were monitored, matching the major isotopes of Cd: ¹¹⁰Cd (12.5%), ¹¹¹Cd (12.8%), ¹¹²Cd (24.1%), ¹¹³Cd (12.2%), and ¹¹⁴Cd (28.8%). A linear correction was applied to the yield to account for frequency-dependent variation in the IR laser pulse energy. These corrections are appropriate for this experiment because the power dependence of the dissociation is practically linear until saturation occurs because of the incoherent nature of the multiple photon process, a phenomenon well detailed in the literature. ²⁶

Computational Details

Low-lying conformers were determined using the Gaussian 16 suite of programs.²⁷ Initial optimizations of the zinc-containing structures were done at the B3LYP/6-31G(d) level of theory using the "loose" keyword to allow a large step size of 0.01 au and a root mean square force constant of 0.0017 to aid convergence. Unique Zn²⁺ complexes were then optimized further at the B3LYP/6-311+G(d,p) level of theory. These optimized structures were used to generate the cadmium containing species by simply replacing the zinc atom with a cadmium atom and reoptimizing using the B3LYP/def2-TZVP basis set, which includes a small core (28 electron) effective core potential (ECP) on the cadmium atom.²⁸⁻²⁹ Both the def2-TZVP basis set and the ECP were obtained from the EMSL basis set exchange.³⁰ Vibrational frequencies obtained from

these optimized structures were scaled by 0.975 for comparison to IRMPD spectra in order to account for known imprecisions in the calculated frequencies and anharmonicity of the vibrational modes. To account for the finite laser bandwidth and unresolved rotational structure, a Gaussian line shape (25 cm⁻¹ FWHM) was used to broaden the calculated frequencies for comparison to the IRMPD spectra.³¹ Previous work indicates that this combination of theory and scaling factors provides an accurate description of the structural information for systems with a similar size and makeup.^{11-14, 16-2115}

Single point energy (SPE) calculations of these optimized geometries were performed at the B3LYP, B3P86, and MP2(full) (where full indicates correlation of all electrons, and abbreviated as MP2 below) levels of theory using the 6-311+G(2d,2p) and def-TZVPP basis sets for the zinc and cadmium containing species, respectively. Zero-point energy (ZPE) corrections were applied to SPEs in order to provide 0 K relative enthalpies. Thermal corrections were calculated to obtain 298 K Gibbs energies by using the rigid rotor/harmonic oscillator approximation with the calculated rotational constants and vibrational frequencies. When used for ZPE and thermal corrections, vibrational frequencies were scaled by 0.989.³² To determine whether the inclusion of dispersion forces affected the calculated geometries and energies, the B3LYP-GD3BJ level of theory, which includes a correction for empirical dispersion, ³³⁻³⁴ was also used to optimize the ion geometry. These structures were then used to calculate SPEs using the larger basis sets detailed above and are included for comparison below.

Results and Discussion.

Nomenclature

Previous work has outlined the nomenclature used to identify these metallated amino acid structures, as illustrated in Figure 1. Their metal-binding sites (N_{α} = amino nitrogen, N_{π} = imidazole "pros" nitrogen, CO = carbonyl oxygen, CO_2^- = both oxygens of a carboxylate) are listed in square brackets, where the first and second sets of brackets indicate the coordination sites of the deprotonated histidine and intact histidine ligands, respectively. If present, a negative sign

is placed next to metal-binding sites to indicate where deprotonation has occurred, or to indicate the original location of a hydrogen atom in a zwitterionic structure. Zwitterions are further identified by listing the location of the protonated site in parentheses after the brackets. When necessary, the binding designation is followed by a description of the dihedral angles in the amino acid conformations using c (cis, 0° - 45°), g (gauche, 45° - 135°), and t (trans, 135° - 180°). The first letter describes the ∠OCCC dihedral angle of the (His-H)⁻ ligand starting at the oxygen closest to the metal center. The three subsequent letters describe the ∠HOCC, ∠OCCC, and ∠CCCC dihedrals for the intact His ligand, starting at the terminal carboxylic acid hydrogen. When needed for zinc species, + and – signs indicate whether the trans angle is positive or negative.

Relative Energies and Structures of Zn Complexes

Table 1 lists the single point enthalpies at 0 K and 298 K Gibbs energies calculated at the B3LYP, B3LYP-GD3BJ, B3P86, and MP2 levels of theory relative to the lowest energy conformer for the zinc complex. For the Zn(His-H)(His)⁺ species, the three density functional theory (DFT) approaches, B3LYP, B3LYP-GD3BJ, and B3P86, predict the ground structure (GS) to be $[N_{\alpha},N_{\pi},CO^-][CO_2^-](N_{\pi}H^+)$, Figure 2. This pentadentate zwitterionic structure is characterized by metal coordination with the (His-H)⁻ ligand at the backbone amine nitrogen, π nitrogen of the imidazole ring, and the deprotonated carbonyl oxygen of the carboxylate. The intact His ligand differs from the classical histidine structure in that the carboxylic acid proton has shifted to the π nitrogen, making it zwitterionic. This allows strong metal binding to both oxygen atoms of the carboxylate group. The complex is stabilized by an inter-ligand hydrogen bond between the hydrogen attached to the π nitrogen and the carboxylate oxygen coordinating with the metal cation on the (His-H)⁻ ligand. MP2 theory places this structure ~5 kJ/mol above its GS.

The MP2 GS is $[N_{\alpha},N_{\pi},CO^{-}][N_{\alpha},N_{\pi}]$ gtgg, Figure 2, which exhibits the same metal coordination sites on the (His-H)⁻ ligand as the DFT GS. In contrast, the intact His ligand is more "canonical" (not zwitterionic) and binds its amine and π nitrogen to the Zn ion. DFT approaches predict this structure to be 2 – 16 kJ/mol higher in energy at 298 K than the GS conformer, Table

1. A similar structure, $[N_{\alpha},N_{\pi},CO^{-}][N_{\alpha},N_{\pi}]$ gtgt, was also found, where the most significant difference with the gtgg analogue is the relative orientation of the carboxylic acid moiety, which allows an $N_{\alpha}H$ •OC hydrogen bond in gtgt. This second conformer is predicted to be 5 – 13 kJ/mol higher in energy than the GS and either ~3 kJ/mol below (B3LYP and B3P86) or 3 – 7 kJ/mol above (B3LYP-GD3BJ and MP2) the gtgg analogue.

The hexadentate $[N_{\alpha},N_{\pi},CO^-][N_{\alpha},N_{\pi},CO]$ conformer was also identified, Figure 2, and is characterized by metal coordination with the amine nitrogen, π nitrogen of the imidazole ring, and the oxygen of the carboxylic acid for both the deprotonated and intact His ligands. Even though this conformer has the metal coordinating with six overall sites, the energy is predicted to be 3 – 23 kJ/mol higher in energy than the five-coordinate GS. The relative energetics of the 5- and 6-coordinate species are consistent with previous spectroscopic experiments that indicate Zn^{2+} favors a coordination number of 5.35 At 17 – 21 kJ/mol above the GS, another zwitterionic structure was found, $[N_{\alpha},N_{\pi},CO^-][CO_2^-](N_{\alpha}H^+)$, where the metal is bound to the same sites as the DFT GS, but the proton on the intact histidine is attached to the amine nitrogen rather than N_{π} . This hydrogen stabilizes the intact His ligand by hydrogen bonding with the π nitrogen of the imidazole ring. Another structure similar to the DFT GS is $[N_{\alpha},N_{\pi},CO^-][N_{\alpha},CO^-](N_{\pi}H^+)$, 13-25 kJ/mol above the GS. Here, the metal is bound to one oxygen and N_{α} in the intact ligand rather than to both carboxylate oxygens. In addition to these six lowest-lying structures, nine other structures were found, as listed in Table 1 and shown in Figure S1. In all but one case, these exhibit four coordinate complexation, such that they lie 15 – 108 kJ/mol above the GS at 298 K.

The six lowest energy structures display a narrow range of metal-ligand bond distances to the coordination sites on the deprotonated histidine: $Zn-N_{\pi}$ (2.03 – 2.12 Å), $Zn-N_{\alpha}$ (2.11 – 2.22 Å), and Zn-O (1.97 – 2.04 Å). This is consistent with the observed binding motif assigned to all six of these structures, $[N_{\alpha},N_{\pi},CO^{-}]$. In these same structures, the intact His ligand samples several different conformations, and therefore reflects a broader range of metal-ligand bond distances. When the coordination site is the amine nitrogen, the intact His ligand samples a similarly narrow range of $Zn-N_{\alpha}$ coordination distances (2.19 – 2.31 Å), slightly longer than those seen in the

deprotonated ligand. For $[CO_2^-]$ coordination, nearly identical Zn-O bond distances of 1.95 and 1.96 Å are observed for one of the two carboxylate oxygens, and the second Zn-O bond length is 2.49 and 3.02 Å for the $(N_{\pi}H^+)$ and $(N_{\alpha}H^+)$ species, respectively. This difference can be attributed to the protonated N_{α} group withdrawing electron density from the carboxylate oxygen via a hydrogen bond. For the hexadentate $[N_{\alpha},N_{\pi},CO^-][N_{\alpha},N_{\pi},CO]$ structure, the Zn-N_{\alpha} and Zn-N_{\alpha} distances are nearly identical in both ligands, whereas the Zn-O coordination distances are 2.04 and 2.89 Å for the deprotonated and intact ligand, respectively. A full tabulation of the metalligand distances of all structures can be found in Table 2

Relative Energies and Structures of Cd Complexes

Table 3 presents the relative energies for Cd(His-H)(His)⁺ structures. The B3LYP and B3P86 GS is $[N_{\alpha},N_{\pi},CO^{-}][CO_{2}^{-}](N_{\pi}H^{+})$, which is a qualitatively similar structure to that of the DFT GSs for the zinc system. The B3LYP-GD3BJ and MP2 levels of theory predict this structure to be 3 – 10 kJ/mol higher in energy than the alternative GS found for this species, $[N_{\alpha},N_{\pi},CO^{-}][N_{\alpha},N_{\pi}]$ gtgg, which B3LYP and B3P86 place ~8 kJ/mol above the GS. The $[N_{\alpha},N_{\pi},CO^{-}][N_{\alpha},N_{\pi},CO]$ hexadentate conformer is also low lying for the cadmium species at 4 – 15 kJ/mol above the GS. All complexes are similar to those shown for the Zn analogues in Figure 2.

In addition to $[N_{\alpha},N_{\pi},CO^{-}][CO_{2}^{-}](N_{\pi}H^{+})$, other zwitterionic species located for $Zn(His-H)(His)^{+}$, $[N_{\alpha},N_{\pi},CO^{-}][N_{\alpha},CO^{-}](N_{\pi}H^{+})$ and $[N_{\alpha},N_{\pi},CO^{-}][CO_{2}^{-}](N_{\alpha}H^{+})$, were also explored for the $Cd(His-H)(His)^{+}$ systems. The $[N_{\alpha},N_{\pi},CO^{-}][N_{\alpha},CO^{-}](N_{\pi}H^{+})$ structure for Cd is 18-29 kJ/mol above the GS, which is only 4-10 kJ/mol higher in energy than the zinc analogue. In contrast, for Cd, the $[N_{\alpha},N_{\pi},CO^{-}][N_{\pi},CO_{2}^{-}](N_{\alpha}H^{+})$ structure is now 51-60 kJ/mol above the GS, an increase of 30-40 kJ/mol compared to the relative energies predicted for the zinc analogue. This change in relative energies could be explained by the change in coordination between the two structures. The zinc structure, $[N_{\alpha},N_{\pi},CO^{-}][CO_{2}^{-}](N_{\alpha}H^{+})$, has the metal center coordinating with both carboxylate oxygens of the intact His ligand; however, when the metal center is changed to

cadmium, it also coordinates with N_{π} of the His ligand. To verify whether an analogous hexadentate structure might exist for the zinc species, the cadmium center in this hexadentate structure was replaced with zinc and recalculated. With a smaller basis set, 6-31G(d), the Zn center maintains its coordination with the N_{π} site, which is consistent with the cadmium structure; however, when optimizing with the 6-311+G(d,p) basis set, the N_{π} site swivels away from the zinc center to form an energetically preferable hydrogen-bond with the $N_{\alpha}H_3^+$ group.

Compared to the six lowest-lying Zn structures, the various conformers of Cd exhibit similar binding motifs, but the metal-ligand bond distances associated with the deprotonated histidine exhibit longer M-N_{π} (by ~0.2 Å), M-N_{α} (by ~0.3 Å), and M-O (by ~0.2 Å) bond distances. These differences can be attributed to the different metal ionic radii (0.60 Å for Zn²⁺ and 0.78 Å for Cd²⁺).¹⁰ A full tabulation of metal-ligand bond distances for the Cd(His-H)(His)⁺ conformers can be found in Table 2.

Additional structures were also located for Cd(His-H)(His)⁺ and can be found in Table 3, with all structures shown in Figure S2. In general, for both the zinc and cadmium species, the relative energies at the B3LYP and B3P86 levels are in accord but differ from those at the B3LYP-GD3BJ and MP2 levels of theory, which agree reasonably well with one another. The relative single point energies predicted by all four levels of theory trend similarly, but the B3LYP-GD3BJ and MP2 predict lower energies than B3LYP and B3P86 for the lowest four conformers for Zn(His-H)(His)⁺ and the lowest three for the Cd(His-H)(His)⁺. Because the GD3BJ empirical dispersion was developed to handle long-range interactions, which are readily apparent in these dimeric structures, it seems possible that the MP2 and B3LYP-GD3BJ values may more accurately describe the relative energetics of each discrete conformer.

Comparison of Experimental and Theoretical Spectra: Zn(His-H)(His)+

Photodissociation of $Zn(His-H)(His)^+$ was monitored from 580 to 1800 cm⁻¹. Parent ions monitored included m/z 373, 374, 375, and 376 for most Zn isotopes. A variety of photodissociation pathways were observed and correspond mainly to losses of H_2O , CO, CO_2 , and

C₆H₇N₃O (His – H₂O). A full list of product ions included in the yield calculation can be found in the Supporting Information Table S1. The IRMPD action spectra presented here correspond to the sum of all product ions as a function of laser wavelength. When comparing IRMPD spectra to the theoretically derived spectra, it is essential to note that their intensities may deviate from one another. Theoretical spectra assume a one-photon absorption process, whereas IRMPD intrinsically requires the absorption of multiple IR photons of a resonant wavelength to induce dissociation.

Figure 3 presents the IRMPD action spectrum of Zn(His-H)(His)⁺ and comparisons to five calculated spectra. Lists of the calculated frequencies and intensities can be found in the Supporting Information Table S2. Major spectral features are centered at 1704, 1585, 1431, 1272, 1144, 1074, 836 (broad) and 596 cm⁻¹, with minor bands present at 1762, 1497, 1180, 1030, 920 (broad), and 664 cm⁻¹. The spectrum for the $[N_{\alpha}, N_{\pi}, CO^{-}][CO_{2}^{-}](N_{\pi}H^{+})$ structure, the DFT GS, reproduces most of the significant features of the experimental spectrum. Specifically bands at 1710 (uncoordinated CO stretch of (His-H) with minor contribution from $N_{\pi}H$ stretch); 1627 and 1607 (N_{α}H₂ scissor), 1622 (N_{π}H rock), 1595 (coordinated CO stretch of His); 1441 and 1446 (sidechain CH₂ symmetric bend); 1301, 1289, 1277, and 1250 (CH and CH₂ motions along the backbone and side-chain); 1143 (N_αH₂ twist); 1066 and 1050 (CN_τC imidazole stretch); 826 (N_αH₂ bend of His); 665 (N_τH out-of-plane bend with minor contributions from N_αH₂ and uncoordinated CO motions of (His-H)⁻) and 660 (N_tH out-of-plane bend of His); 598 and 583 cm⁻¹ (imidazole outof-plane bend). This structure also has a predicted band of modest intensity at 1354 cm⁻¹ (coordinated CO stretch of (His-H) with contributions from the backbone CH motion), which could be the blue tail on the spectral feature observed at 1272 cm⁻¹. The hydrogen attached to the intact His ligand N_{π} , a defining feature of this structure, is predicted to contribute to a band at 1052 cm⁻¹, which also includes the out-of-plane $N_{\alpha}H_2$ bending from the (His-H)⁻ ligand. Experimentally, this narrow band appears at 1074 cm⁻¹.

Probably the main discrepancies between these two spectra are that this calculated spectrum lacks the experimentally observed intensity between 1510 and 1580 cm⁻¹ and at 1431

cm⁻¹. In previous studies of metallated amino acids, the $N_{\alpha}H_2$ scissor motion was observed at frequencies lower than those predicted by 22-42 cm⁻¹, a consequence of this motion being strongly anharmonic. ^{11, 13-16, 26, 36-3912} Such a shift in the $N_{\alpha}H_2$ scissor bands predicted at 1607 and 1627 cm⁻¹ would reproduce the intensity near 1560-1580 cm⁻¹ observed in the IRMPD spectrum. Such anharmonic effects may also be needed to explain the strong experimental band centered at 1431 cm⁻¹. If bands predicted at 1442 and 1447 (CH₂ bends) and minor bands at 1448 and 1456 cm⁻¹ ($N_{\tau}H$ in-plane bend) were redshifted by ~20 cm⁻¹, they could match the experimental band although with a lower intensity than observed. Previous work has shown that linear absorption calculations may not account for the intensity of the bands located in this area. ¹¹

To explore these anharmonic effects, additional anharmonic frequency calculations were performed for imidazole and the $[N_{\alpha},N_{\pi},CO^{-}][CO_{2}^{-}](N_{\pi}H^{+})$ structure at the B3LYP/6-311+G(d,p) level (using the keyword "freq=anharmonic"). The imidazole calculation predicts a harmonic $N_{\tau}H$ bending motion at 1430 cm⁻¹ with the anharmonic band redshifted to 1385 cm⁻¹. As hypothesized above, this anharmonic shift is larger than for most other modes of the model molecule, although the scaling factor often applied to harmonic calculations (0.975 in the present case) accounts for much of this effect (1394 cm⁻¹ scaled harmonic frequency). The anharmonic calculation does not indicate any significant change in the relative intensity of this band (16 vs. 14 km/mol).

Figure S3 compares the experimental IRMPD spectrum with the scaled harmonic and unscaled anharmonic spectra calculated for the $[N_{\alpha},N_{\pi},CO^{-}][CO_{2}^{-}](N_{\pi}H^{+})$ structure. The two spectra are fairly similar, although the anharmonic spectrum reproduces the width of the experimental band at 1704 cm⁻¹ better. Interestingly, the four most intense anharmonic bands in this region are combination bands arising from coupled NH₂ and CH motions (1719, 1697, and 1678 cm⁻¹) and coupled NH₂ and N_{π}H motions (1703 cm⁻¹). The uncoordinated CO stretch present at 1710 cm⁻¹ in the scaled harmonic spectrum is found at 1725 cm⁻¹ but with only 2% of its harmonic intensity. The series of anharmonic bands between 1550 and 1650 cm⁻¹ recreate the experimental feature centered at 1585 cm⁻¹, although shifted to somewhat higher frequencies. The experimental band at 1431 cm⁻¹ remains poorly reproduced in both the harmonic and anharmonic

spectra, and both still predict rather intense bands near 1360 cm⁻¹, for which there is no experimental evidence.

Figure 3 also presents a comparison between the IRMPD spectrum and the $[N_{\alpha},N_{\pi},CO^-][N_{\alpha},N_{\pi}]$ gtgg conformer, the MP2 GS. The higher energy gtgt isomer has a similar spectrum and is compared to the experimental IRMPD spectrum in the Supporting Information Figure S4. Both species reproduce several features present in the experimental spectrum and, except for the band at ~1760 cm⁻¹, are similar to the $[N_{\alpha},N_{\pi},CO^-][CO_2^-](N_{\pi}H^+)$ calculated spectrum, which is consistent with their largely similar binding motif on the $(His-H)^-$ ligand. Both $[N_{\alpha},N_{\pi},CO^-][N_{\alpha},N_{\pi}]$ structures predict a fairly intense band for the uncoordinated CO stretch on the intact His ligand at 1759 (gtgg) and 1767 (gtgt) cm⁻¹, for which there is minor experimental evidence. The observed IRMPD feature at 1762 cm⁻¹ could be indicative of a small population of a $[N_{\alpha},N_{\pi},CO^-][N_{\alpha},N_{\pi}]$ species. The main difference between the spectra of these two isomers is the location of a moderately intense band (C-OH bending) at 1145 (gtgg) and 1157 (gtgt) cm⁻¹, with the lower energy gtgg isomer agreeing better with the experimental band centered at 1139 cm⁻¹. Again these structures do not reproduce the observed intensities near 1431 and 1570 cm⁻¹.

An equilibrium distribution of conformers at 298 K indicates that the $[N_{\alpha},N_{\pi},CO^{-}][CO_{2}^{-}](N_{\pi}H^{+})$ is the dominant species (>99%) at the B3LYP and B3P86 levels of theory. Populations of the $[N_{\alpha},N_{\pi},CO^{-}][CO_{2}^{-}](N_{\pi}H^{+})$ and $[N_{\alpha},N_{\pi},CO^{-}][N_{\alpha},N_{\pi}]$ gtgg conformers are calculated to be 71 and 29%, respectively, at the B3LYP-GD3BJ level of theory and 11 and 89%, respectively, at the MP2 level. Composite spectra using these percentages are compared to the experimental spectra in the supplementary material (Figure S5). These comparisons are consistent with the $[N_{\alpha},N_{\pi},CO^{-}][CO_{2}^{-}](N_{\pi}H^{+})$ species being the dominant contributor to the IRMPD spectrum, with a minor contribution from the $[N_{\alpha},N_{\pi},CO^{-}][N_{\alpha},N_{\pi}]$ gtgg conformer, as suggested by the small band observed at 1765 cm⁻¹.

For completeness, Figure 3 also compares spectra for the hexadentate $[N_{\alpha},N_{\pi},CO^{-}][N_{\alpha},N_{\pi},CO]$ and the zwitterionic $[N_{\alpha},N_{\pi},CO^{-}][CO_{2}^{-}](N_{\alpha}H^{+})$ and $[N_{\alpha},N_{\pi},CO^{-}][N_{\alpha},CO^{-}](N_{\pi}H^{+})$ conformers with the experimental action spectrum. The hexadentate conformer predicts

an intense band at 1759 cm⁻¹ as well as a doublet feature centered at 600 cm⁻¹, neither of which are meaningfully present in the experimental spectrum. Both zwitterionic conformers recreate the intense features at 1704 and 1272 cm⁻¹, but otherwise do not reproduce the experimental spectrum as well as either $[N_{\alpha},N_{\pi},CO^{-}][CO_{2}^{-}](N_{\pi}H^{+})$ or $[N_{\alpha},N_{\pi},CO^{-}][N_{\alpha},N_{\pi}]$ gtgg. In addition, these species still do not reproduce the observed intensities near 1431 and 1570 cm⁻¹. Further, the relative energetics of both zwitterionic species are 17-21 and 13-25 kJ/mol higher in energy than either GS, which suggests populations of both conformers are negligible.

Comparison of Experimental and Theoretical Spectra Cd(His-H)(His)⁺

Photodissociation of Cd(His-H)(His)⁺ was monitored from 570 to 1800 cm⁻¹, and the results are shown in Figure 4. Parent ions monitored included m/z 419, 420, 421, 422, and 423, which includes all major Cd isotopes. Observed dissociation pathways are similar to those observed for the zinc species and are listed in the Supporting Information Table S1. Overall the spectrum for Cd(His-H)(His)⁺ is quite similar to that for the Zn complex, indicating similar binding motifs. Major spectral features are found at 1696, 1562, 1433, 1286, 1140, 1071, and 1023 cm⁻¹, with a broad band from 750 – 900 cm⁻¹ and another band peaking near the 570 cm⁻¹ cutoff. Figure 4 compares the experimental spectrum with those calculated for the five lowest energy conformations. Lists of the calculated frequencies and intensities can be found in the Supporting Information Table S3. The $[N_{\alpha},N_{\pi},CO^{-}][CO_{2}^{-}](N_{\pi}H^{+})$ isomer (B3LYP and B3P86 GS) reproduces several observed spectral features. Namely, predicted bands are found at 1681 (uncoordinated CO stretch of (His-H)⁻ with a minor contribution from $N_{\pi}H$ stretch); 1628 and 1599 ($N_{\alpha}H_2$ scissor); 1623 ($N_{\pi}H$ rock); 1551 and 1383 (coordinated CO stretch of His); 1295 and 1282 (coordinated CO stretch of His with CH and CH₂ motions along the backbone and side-chain); 1156 and 1146 ($N_{\alpha}H_2$ twisting); and 1031 (out-of-plane $N_{\alpha}H_2$ bending). Similar to the $[N_{\alpha},N_{\pi},CO^-][CO_2^-](N_{\pi}H^+)$ zinc isomer, the band predicted at 1078 cm⁻¹ is indicative of a hydrogen bound to the N_{π} of the intact His ligand, which agrees well with the sharp feature observed at 1071 cm⁻¹. The anharmonic effects leading to a red-shift in the bands associated with the N_αH₂ scissor motion mentioned above would contribute to the broad spectral feature centered at 1562 cm^{-1} , which is dominated by the predicted band at 1551 cm^{-1} . The shoulder on this band at 1496 cm^{-1} is reproduced by the C-N_{π}-C stretch predicted for this conformer at 1494 cm^{-1} . As for the Zn analogue, the major band observed at 1433 cm^{-1} is not reproduced by this species, but again, redshifted bands predicted for backbone CH₂ motions and N_{τ}H bends $(1454 - 1437 \text{ cm}^{-1})$ may explain this observation.

 $[N_{\alpha},N_{\pi},CO^{-}][N_{\alpha},N_{\pi}]$ gtgg, the GS at the B3LYP-GD3BJ and MP2 levels of theory, is also compared to the experimental IRMPD spectrum in Figure 4. This conformation, unlike the $[N_{\alpha},N_{\pi},CO^{-}][CO_{2}^{-}](N_{\pi}H^{+})$ isomer, recreates the high frequency shoulder on the feature centered at 1696 cm⁻¹ and is assigned to the uncoordinated CO stretch of the (His-H)⁻ ligand at 1755 cm⁻¹. Other predicted bands are found at 1701 (uncoordinated CO stretch of His ligand); 1293 (coordinated CO and $N_{\alpha}H_{2}$ with minor contributions from backbone stretching); and 1027 cm⁻¹ $(N_{\alpha}H_{2} \text{ out-of-plane wagging from His and (His-H)}^{-} \text{ ligands})$. The bands predicted at 1143 and 1140 (C-OH bend, $N_{\alpha}H_{2}$ twisting, and $CN_{\tau}C$ imidazole stretch) recreate the spectral feature at 1140 cm⁻¹ very well.

The B3LYP-GD3BJ and MP2 basis sets also predict a low-lying (4 - 6 kJ/mol) $[N_{\alpha},N_{\pi},CO^{-}][N_{\alpha},N_{\pi},CO]$ isomer, which has a spectrum similar to that for the $[N_{\alpha},N_{\pi},CO^{-}][N_{\alpha},N_{\pi}]$ gtgg isomer with the addition of a more intense band at 997 cm⁻¹ $(N_{\alpha}H_{2} \text{ out-of-plane wagging from His ligand})$. As seen in the zinc system, the spectrum for the gtgt isomer was also found to be similar to that of gtgg and is shown in Figure S3. An equilibrium distribution at 298 K of the $[N_{\alpha},N_{\pi},CO^{-}][CO_{2}^{-}](N_{\pi}H^{+})$, $[N_{\alpha},N_{\pi},CO^{-}][N_{\alpha},N_{\pi}]$ gtgg, and $[N_{\alpha},N_{\pi},CO^{-}][N_{\alpha},N_{\pi},CO]$ species at the MP2 level predicts conformer populations of 2%, 85%, and 13%, respectively, whereas B3LYP-GD3BJ predicts a distribution of 17%, 75%, and 8%, and B3LYP and B3P86 suggest 97%, 3%, <1% and 95%, 4%, and <1%, respectively. See Figure S6 for weighted spectra compared to the experimental IRMPD spectrum.

Conformers $[N_{\pi},CO_2^-][N_{\alpha},N_{\pi},CO]$ and $[N_{\alpha},N_{\pi},CO^-][N_{\alpha},CO^-](N_{\pi}H^+)$ are also compared to the experimental spectrum in Figure 4. The former species could only be a minor contributor to experiment given its intense band at 1741 cm⁻¹, but is unlikely because it lies 16-25 kJ/mol above

either GS. As seen for the zinc system, $[N_{\alpha},N_{\pi},CO^{-}][N_{\alpha},CO^{-}](N_{\pi}H^{+})$ is neither energetically favorable, nor does it predict the IRMPD spectrum as well as the spectrum of the GS. Similar to the Zn system, we conclude that $[N_{\alpha},N_{\pi},CO^{-}][CO_{2}^{-}](N_{\pi}H^{+})$ is the dominant species contributing to the experimental spectrum, but minor contributions from the $[N_{\alpha},N_{\pi},CO^{-}][N_{\alpha},N_{\pi}]$ gtgg and/or $[N_{\alpha},N_{\pi},CO^{-}][N_{\alpha},N_{\pi},CO^{-}]$ conformers are suggested by the intensity observed at 1765 cm⁻¹.

Comparison to $M(His-H)^+$ and $M^{2+}(His)_2$

Previous IRMPD experiments by Hofstetter et al. have studied the metal-ligand coordination of zinc and cadmium dications with a single deprotonated histidine (His-H)⁻ and two intact histidine ligands over a similar wavelength range. Strong spectral evidence supports tridentate [N $_{\alpha}$,N $_{\pi}$,CO⁻] metal-ligand coordination for the M(His-H)⁺ complexes. These complexes are qualitatively similar to the low-lying conformations adopted by the (His-H)⁻ ligand of the M(His-H)(His)⁺ complexes examined here. The relative theoretical energies indicate that this is the preferred binding motif of the (His-H)⁻ ligand for both Zn²⁺ and Cd²⁺.

The structures that were calculated for the previously explored M²⁺(His)₂ systems indicate a preference by DFT levels of theory for one of the histidine ligands to exhibit a charge-solvated (CS) structure while the other exhibits a salt-bridge (SB) conformation. In the present study, a similar preference by DFT levels of theory is observed for M(His-H)(His)⁺, with the exception being that B3LYP-GD3BJ predicts a CS/CS structure for the Cd species. For both the metallated dimer and M(His-H)(His)⁺ systems, the MP2 level of theory indicates a strong preference for CS/CS binding. The similarities between these two systems, especially in regards to the ligating species and metal centers, mean it is not surprising that theory predicts very similar trends.

Spectral identification of the $M^{2+}(His)_2$ system indicated that at least one of the His ligands was in its canonical form, but whether the other His ligand adopted a zwitterionic conformation was ambiguous. Relative theoretical energies calculated at the B3LYP and MP2 levels did not indicate a clear preference for a specific structure. The $Cd^{2+}(His)_2$ spectrum seemed to agree best with the identified hexadentate structure, which is similar to that of the $[N_{\alpha}, N_{\pi}, CO^{-}][N_{\alpha}, N_{\pi}, CO]$

structure presented here (a possible contributor to the observed IRMPD spectrum for the $Cd(His-H)(His)^+$ species). Interestingly, a comparison of the IRMPD spectra of the $M^{2+}(His)_2$ and $M(His-H)(His)^+$ species shows that the former species has several more bands than the latter across the 600-1800 cm⁻¹ range. These additional bands contributed to the difficulty in assigning the presence of specific conformers for the dimeric species, and are a result of mismatches in intensity, anharmonic effects, multiple conformations present, or some combination of these effects, as mentioned above. A similar investigation of the $M^{2+}(Trp)_2$ (M = Zn, Ca, Sr, Ba, Mn, Co, and Cd) systems revealed evidence for one canonical and one zwitterionic ligand, whereas $Ni^{2+}(Trp)_2$ uniquely was identified to have both ligands in a canonical form. $^{40-41}$ The identified $M^{2+}(Trp)_2$ conformers did not exhibit intramolecular ligand coordination, as seen for the $M(His-H)(His)^+$ species, which might be relevant in explaining earlier observations that zinc plays a role in the aggregation of $A\beta$ peptides. $^{4-5}$

Nair et al. also studied Zn^{2+} complexed with two histidine amino acids using proton NMR.⁴² The $Zn(His)_2$ complex was determined to adopt an octahedral-like, hexadentate structure, where the Zn is bound to the N_{α} , N_{π} , and CO groups of both histidine amino acids. This type of coordination would be similar to the $[N_{\alpha},N_{\pi},CO^-][N_{\alpha},N_{\pi},CO]$ structure found in the present computational survey. The spectral comparison indicates that, at least in the gas-phase, this structure is not a significant contributor to the observed species for the Zn species. The $Cd(His-H)(His)^+$ species, on the other hand, has some spectral characteristics that indicate a possible contribution from this hexadentate structure.

Relative Conformer Stability Predictions using DFT Methods and MP2

From the above discussions, it is clear that the MP2 level of theory, combined with the basis sets used here, appears to incorrectly predict the dominant conformations observed in the IRMPD spectra for both metallated species. As we have now examined a fair number of functionalized amino acids (eleven) complexed with Zn and Cd, it may be worth reviewing whether there is a best level of theory to use for such complexes (as suggested by a referee). For many of these systems (Cys, 12 Met, 21 Lys, 19 Asp and Asp dimer, 17 Asn, 15 Glu, 16 Gln, 13 and one

His ligand¹¹), both DFT and MP2 approaches predict the same ground structure, which then accurately reproduces the observed IR spectra. In our study of Ser and Thr complexes, 14, 20 all levels of theory agreed for the CdCl⁺(Ser) complex, but for [Zn(Ser-H)ACN]⁺ (where ACN = acetonitrile), DFT predicted deprotonation at the hydroxyl side chain is preferred, whereas MP2 indicated the carboxylic acid was deprotonated. Spectral analysis indicated that both conformations were present, but that the latter isomer dominated, consistent with the MP2 prediction. For the comparable [Zn(Thr-H)ACN]⁺ complex, the additional methyl group shifts the relative energies of the two deprotonation sites to favor the carboxylic acid, which is now predicted to be the ground structure by B3LYP, B3LYP-GD3BJ, and MP2 (but not B3P86), and this species is confirmed to be the correct ground state spectroscopically. For Arg, ¹⁸ now all levels of theory agree on the [Zn(Arg-H)]⁺ ground structure, but the CdCl⁺(Arg) spectrum is accurately predicted by B3LYP-GD3BJ and MP2 levels, but not by B3LYP and B3P86 as these predict a zwitterionic structure that may be present but is clearly not the dominant species formed experimentally. Finally, although CdCl(His)⁺, [Cd(His-H)]⁺, and [Zn(His-H)]⁺ complexes were accurately predicted by both B3LYP and MP2 theory, predictions for the M²⁺(His)₂ systems (discussed above) differ between the two approaches, with MP2 greatly preferring a CS/CS structure and B3LYP suggesting CS/SB ligation. 11 As noted above, the complexity of these spectra did not allow an unambiguous assignment, although the Cd²⁺(His)₂ spectrum looked more like the CS/CS spectrum (the MP2 ground structure) than the CS/SB spectrum and the Zn²⁺(His)₂ spectrum was very similar. Overall, it is clear that DFT and MP2 differ in their assessment of zwitterionic stability, but it appears that the failure of MP2 to correctly predict the correct ground structure of the M(His-H)(His)⁺ systems is not a robust result. We believe it remains prudent to calculate relative energies at the B3LYP (which B3P86 generally matches), B3LYP-GD3BJ, and MP2 levels of theory, although other approaches not considered here may also be useful.

Conclusions

Action spectroscopy was used to measure the IRMPD spectra of M(His-H)(His)⁺ (M = Zn and Cd) from 580 - 1800 cm⁻¹. The resultant spectra were compared with theoretical IR spectra calculated at the B3LYP/6-311+G(d,p) and B3LYP/def2-TZVP levels for the Zn and Cd species, respectively. Good agreement between theory and experiment was observed for the Zn(His-H)(His)⁺ complex, where the $[N_{\alpha},N_{\pi},CO^{-}][CO_{2}^{-}](N_{\pi}H^{+})$ structure predicts the experimental spectrum well, with a small contribution from $[N_{\alpha},N_{\pi},CO^{-}][N_{\alpha},N_{\pi}]$ gtgg likely. For Cd(His-H)(His)⁺, the $[N_{\alpha},N_{\pi},CO^{-}][CO_{2}^{-}](N_{\pi}H^{+})$ explains the majority of the recorded spectrum, with possible contributions from $[N_{\alpha},N_{\pi},CO^{-}][N_{\alpha},N_{\pi}]$ gtgg and/or $[N_{\alpha},N_{\pi},CO^{-}][N_{\alpha},N_{\pi},$

Overall, the theoretical methods described here disagree about the relative energetics of the low-lying structures. All levels of theory indicate a tridentate $[N_{\alpha},N_{\pi},CO^-]$ binding character for the (His-H)⁻ ligand, independent of metal identity. For the Zn system, all four levels of theory predicted a pentadentate GS, which is consistent with previous work that indicates Zn has a coordination number of five.³⁵ The DFT levels of theory indicate a preference for a zwitterionic GS that is more consistent with experiment, whereas the MP2 level of theory predicts a canonical GS. This difference is consistent with previous observations that MP2 disfavors zwitterionic systems.^{11, 18}

For the Cd species, the B3LYP and B3P86 levels of theory predict a zwitterionic GS that matches that of the Zn species, whereas the B3LYP-GD3BJ and MP2 GS predict the canonical structure, $[N_{\alpha},N_{\pi},CO^{-}][N_{\alpha},N_{\pi}]$ gtgg. This second structure was predicted to be the GS for both metallated systems at the MP2 level of theory, and to be <4 kJ/mol higher at the B3LYP-GD3BJ level of theory when metallated with Cd. Again, the DFT results are more consistent with experiment. Spectral comparison indicates that the Cd system could potentially exhibit more flexibility in favored coordination, where the presence of both a penta- and hexadentate ligation could possibly explain the observed bands. To complete an analysis of the metal-binding characteristics of the (His-H)(His) system, it would be worthwhile to expand to additional M(His-

H)(His)⁺ species to determine the spectral, energetic, and conformational preferences of this histidine dimer system in regards to metal identity.

Supporting Information

Tables showing observed fragmentation products and IR vibrational frequencies and intensities of low-lying conformers. Figures showing additional structures for $Zn(His-H)(His)^+$ and $Cd(His-H)(His)^+$, comparison of harmonic and anharmonic spectra for the $Zn(His-H)(His)^+$ $[N_{\alpha},N_{\pi},CO^-][CO_2^-](N_{\pi}H^+)$ structure, theoretical spectra for $[N_{\alpha},N_{\pi},CO^-][N_{\alpha},N_{\pi}]$ gtgt isomers compared to IRMPD spectra for both metal systems, and composite spectra of theoretical conformer distributions.

Acknowledgments

Financial support for this work was provided by the National Science Foundation, Grant CHE-1954142. MS thanks the German Science Foundation, Grant SCHA 871-10/1 for financial support and Dr. Katrin Peckelsen for initial experiments and results. The authors gratefully acknowledge the *Nederlandse Organisatie voor Wetenschappelijk Onderzoek* (NWO) for the support of the FELIX Laboratory. We also appreciate a generous grant of computer time from the Center of High Performance Computing at the University of Utah.

References

- 1. Coleman, J. E., Zinc proteins: enzymes, storage proteins, transcription factors, and replication proteins. *Annu. Rev. Biochem.* **1992**, *61*, 897-946.
- 2. Miller, J.; McLachlan, A.; Klug, A., Repetitive zinc-binding domains in the protein transcription factor IIIA from Xenopus oocytes. *EMBO J.* **1985,** *4*, 1609-1614.
- 3. Mackay, J. P.; Crossley, M., Zinc Fingers are Sticking Together. *Trends Biochem. Sci.* **1998,** *23*, 1-4.
- 4. Esler, W. P.; Stimson, E. R.; Jennings, J. M.; Ghilardi, J. R.; Mantyh, P. W.; Maggio, J. E., Zinc-induced aggregation of human and rat β-amyloid peptides in vitro. *J. Neurochem.* **1996**, *66*, 723-732.
- 5. Bush, A. I.; Pettingell, W. H.; Multhaup, G.; d Paradis, M.; Vonsattel, J.-P.; Gusella, J. F.; Beyreuther, K.; Masters, C. L.; Tanzi, R. E., Rapid induction of Alzheimer Aβ amyloid formation by zinc. *Science* **1994**, *265*, 1464-1467.

- 6. Suzuki, K.; Miura, T.; Takeuchi, H., Inhibitory effect of copper (II) on zinc (II)-induced aggregation of amyloid β-peptide. *Biochem. Biophys. Res. Commun.* **2001**, *285*, 991-996.
- 7. Cragnell, C.; Staby, L.; Lenton, S.; Kragelund, B. B.; Skepö, M., Dynamical oligomerisation of histidine rich intrinsically disordered proteins is regulated through zinchistidine interactions. *Biomolecules* **2019**, *9*, 168.
- 8. Istrate, A. N.; Kozin, S. A.; Zhokhov, S. S.; Mantsyzov, A. B.; Kechko, O. I.; Pastore, A.; Makarov, A. A.; Polshakov, V. I., Interplay of histidine residues of the Alzheimer's disease Aβ peptide governs its Zn-induced oligomerization. *Sci. Rep.* **2016**, *6*, 1-14.
- 9. Peckelsen, K.; Martens, J.; Berden, G.; Oomens, J.; Dunbar, R. C.; Meijer, A. J. H. M.; Schäfer, M., Gas-phase Complexes of Ni²⁺ and Ca²⁺ with Deprotonated Histidylhistidine (HisHis): A Model Case for Polyhistidyl-metal Binding Motifs. *J. Mol. Spec.* **2017**, *332*, 38-44.
- 10. Shannon, R. D., Revised Effective Ionic Radii and Systematic Studies of Interatomic Distances in Halides and Chalcogenides. *Acta Cryst.* **1976**, *A32*, 751-767.
- 11. Hofstetter, T. E.; Howder, C.; Berden, G.; Oomens, J.; Armentrout, P. B., Structural Elucidation of Biological and Toxicological Complexes: Investigation of Monomeric and Dimeric Complexes of Histidine with Multiply Charged Transition Metal (Zn and Cd) Cations using IR Action Spectroscopy. *J. Phys. Chem. B* **2011**, *115*, 12648-12661.
- 12. Coates, R. A.; McNary, C. P.; Boles, G. C.; Berden, G.; Oomens, J.; Armentrout, P. B., Structural Characterization of Gas-Phase Cysteine and Cysteine Methyl Ester Complexes with Zinc and Cadmium Dications by Infrared Multiple Photon Dissociation Spectroscopy. *Phys. Chem. Chem. Phys.* **2015**, *17*, 25799-25808.
- 13. Boles, G. C.; Coates, R. A.; Berden, G.; Oomens, J.; Armentrout, P. B., Experimental and Theoretical Investigations of Infrared Multiple Photon Dissociation Spectra of Glutamine Complexes with Zn²⁺ and Cd²⁺. *J. Phys. Chem. B* **2015**, *119*, 11607–11617.
- 14. Coates, R. A.; Boles, G. C.; McNary, C. P.; Berden, G.; Oomens, J.; Armentrout, P. B., Zn²⁺ and Cd²⁺ Cationized Serine Complexes: Infrared Multiple Photon Dissociation Spectroscopy and Density Functional Theory Investigations. *Phys. Chem. Chem. Phys.* **2016**, *18*, 22434 22445.
- 15. Boles, G. C.; Coates, R. A.; Berden, G.; Oomens, J.; Armentrout, P. B., Experimental and Theoretical Investigations of Infrared Multiple Photon Dissociation Spectra of Asparagine Complexes with Zn²⁺ and Cd²⁺ and Their Deamidation Processes. *J. Phys. Chem. B* **2016**, *120*, 12486-12500.
- 16. Boles, G. C.; Owen, C. J.; Berden, G.; Oomens, J.; Armentrout, P. B., Experimental and Theoretical Investigations of Infrared Multiple Photon Dissociation Spectra of Glutamic Acid Complexes with Zn²⁺ and Cd²⁺. *Phys. Chem. Chem. Phys.* **2017**, *19*, 12394 12406.
- 17. Boles, G. C.; Hightower, R. L.; Coates, R. A.; McNary, C. P.; Berden, G.; Oomens, J.; Armentrout, P. B., Experimental and Theoretical Investigations of Infrared Multiple Photon Dissociation Spectra of Aspartic Acid Complexes with Zn²⁺ and Cd²⁺. *J. Phys. Chem. B* **2018**, *122*, 3836-3853.
- 18. Chalifoux, A. M.; Boles, G. C.; Berden, G.; Oomens, J.; Armentrout, P. B., Experimental and Theoretical Investigations of Infrared Multiple Photon Dissociation Spectra of Arginine Complexes with Zn²⁺ and Cd²⁺. *Phys. Chem. Chem. Phys.* **2018**, *20*, 20712-20725.
- 19. Owen, C. J.; Boles, G. C.; Berden, G.; Oomens, J.; Armentrout, P. B., Experimental and Theoretical Investigations of Infrared Multiple Photon Dissociation Spectra of Lysine Complexes with Zn²⁺ and Cd²⁺. *Eur. J. Mass Spectrom.* **2019**, *25*, 97-111.

- 20. Boles, G. C.; Hightower, R. L.; Berden, G.; Oomens, J.; Armentrout, P. B., Zinc and Cadmium Complexation of l-Threonine: An Infrared Multiple Photon Dissociation Spectroscopy and Theoretical Study. *J. Phys. Chem. B* **2019**, *123*, 9343-9354.
- 21. Boles, G. C.; Stevenson, B. C.; Hightower, R. L.; Berden, G.; Oomens, J.; Armentrout, P. B., Zinc and cadmium complexation of L-methionine: An infrared multiple photon dissociation spectroscopy and theoretical study. *J. Mass Spectrom.* **2020**, *n/a*, e4580.
- 22. Ke, S. Y.; Wang, C. C.; Lee, G. H.; Chuang, Y. C.; Lu, K. L., Highly Thermal-Stable Supramolecular Assembly of a Hydrogen-Bonded Mononuclear Nickel (II) Histidine Compound. *J. Chinese Chem. Soc.* **2013**, *60*, 807-812.
- 23. Oepts, D.; van der Meer, A. F. G.; van Amersfoort, P. W., The Free-Electron-Laser User Facility FELIX. *Infrared Phys. Technol.* **1995**, *36*, 297-308.
- 24. Martens, J.; Berden, G.; Gebhardt, C. R.; Oomens, J., Infrared ion spectroscopy in a modified quadrupole ion trap mass spectrometer at the FELIX free electron laser laboratory. *Rev. Sci. Instrum.* **2016**, *87*, 103108.
- 25. Berden, G.; Derksen, M.; Houthuijs, K. J.; Martens, J.; Oomens, J., An Automatic Variable Laser Attenuator for IRMPD Spectroscopy and Analysis of Power-dependence in Fragmentation Spectra. *Int. J. Mass Spectrom.* **2019**, *443*, 1-8.
- 26. Lemaire, J.; Boissel, P.; Heninger, M.; Mauclaire, G.; Bellec, G.; Mestdagh, H.; Le Caer, S.; Ortega, J.; Glotin, F.; Maître, P., Gas Phase Infrared Spectroscopy of Selectively Prepared Ions. *Phys. Rev. Lett.* **2002**, *89*, 273002.
- 27. Frisch, M. J.; Trucks, G. W.; Schlegel, H. B.; Scuseria, G. E.; Robb, M. A.; Cheeseman, J. R.; Scalmani, G.; Barone, V.; Petersson, G. A.; Nakatsuji, H., et al. *Gaussian 16, Revision A.03*, Gaussian, Inc.: Wallingford CT, 2016.
- 28. Andrae, D.; Haeussermann, U.; Dolg, M.; Stoll, H.; Preuss, H., Energy-adjusted Ab Initio Pseudopotentials for the Second and Third Row Transition Elements. *Theor. Chim. Acta* **1990**, 77, 123-141.
- 29. Weigend, F.; Ahlrichs, R., Balanced Basis Sets of Split Valence, Triple Zeta Valence and Quadruple Zeta Valence Quality for H to Rn: Design and Assessment of Accuracy. *Phys. Chem. Phys.* **2005**, *7*, 3297-3305.
- 30. Feller, D., The Role of Databases in Support of Computational Chemistry Calculations. *J. Comput. Chem.* **1996**, *17*, 1571-1586.
- 31. Polfer, N. C., Infrared Multiple Photon Dissociation Spectroscopy of Trapped Ions. *Chem. Soc. Rev.* **2011**, *40*, 2211–2221.
- 32. Kesharwani, M. K.; Brauer, B.; Martin, J. M. L., Frequency and Zero-Point Vibrational Energy Scale Factors for Double-Hybrid Density Functionals (and Other Selected Methods): Can Anharmonic Force Fields Be Avoided? *J. Phys. Chem. A* **2015**, *119*, 1701-1714.
- 33. Grimme, S.; Ehrlich, S.; Goerigk, L., Effect of the Damping Function in Dispersion Corrected Density Functional Theory. *J. Comput. Chem.* **2011**, *32*, 1456-1465.
- 34. Grimme, S.; Antony, J.; Ehrlich, S.; Krieg, H., A Consistent and Accurate Ab Initio Parametrization of Density Functional Dispersion Correction (DFT-D) for the 94 Elements H-Pu. *J. Chem. Phys.* **2010**, *132*, 154104-154119.
- 35. Cooper, T. E.; O'Brien, J. T.; Williams, E. R.; Armentrout, P. B., Zn²⁺ has a Primary Hydration Sphere of Five: IR Action Spectroscopy and Theoretical Studies of Hydrated Zn²⁺ Complexes. *J. Phys. Chem. A* **2010**, *114*, 12646–12655.

- 36. Armentrout, P. B.; Rodgers, M. T.; Oomens, J.; Steill, J. D., Infrared Multiphoton Dissociation Spectroscopy of Cationized Serine: Effects of Alkali-Metal Cation Size on Gas-Phase Conformation. *J. Phys. Chem. A* **2008**, *112*, 2248-2257.
- 37. Rodgers, M. T.; Armentrout, P. B.; Oomens, J.; Steill, J. D., Infrared Multiphoton Dissociation Spectroscopy of Cationized Threonine: Effects of Alkali-Metal Cation Size on Gas-Phase Conformation. *J. Phys. Chem. A* **2008**, *112*, 2258-2267.
- 38. Citir, M.; Hinton, C. S.; Oomens, J.; Steill, J. D.; Armentrout, P. B., Infrared Multiple Photon Dissociation Spectroscopy of Cationized Histidine: Effects of Metal Cation Size on Gas-Phase Conformation. *J. Phys. Chem. A* **2012**, *116*, 1532-1541.
- 39. Citir, M.; Stennett, E. M. S.; Oomens, J.; Steill, J. D.; Rodgers, M. T.; Armentrout, P. B., Infrared Multiple Photon Dissociation Spectroscopy of Cationized Cysteine: Effects of Metal Cation Size on Gas-Phase Conformation. *Int. J. Mass Spectrom.* **2010**, *297*, 9-17.
- 40. Dunbar, R. C.; Steill, J. D.; Polfer, N. C.; Oomens, J., Dimeric Complexes of Tryptophan with M²⁺ Metal Ions. *J. Phys. Chem. A* **2009**, *113*, 845-851.
- 41. Mino, W. K.; Szczepanski, J.; Pearson, W. L.; Powell, D. H.; Dunbar, R. C.; Eyler, J. R.; Polfer, N. C., Vibrational signatures of zwitterionic and charge-solvated structures for alkaline earth-tryptophan dimer complexes in the gas phase. *Int. J. Mass Spectrom.* **2010**, *297*, 131-138.
- 42. Nair, N. G.; Perry, G.; Smith, M. A.; Reddy, V. P., NMR studies of zinc, copper, and iron binding to histidine, the principal metal ion complexing site of amyloid-β peptide. *J. Alzheimer's Disease* **2010**, *20*, 57-66.

Table 1. Relative Enthalpies (0 K) and Gibbs Energies (298 K) of Zn(His-H)(His)⁺ Complexes in kJ/mol^a

Structure	B3LYP		B3LYP-GD3BJ ^b		B3P86		MP2(full)	
$N_{\alpha}, N_{\pi}, CO^{-}][CO_{2}^{-}](N_{\pi}H^{+})$	0.0	(0.0)	0.0	(0.0)	0.0	(0.0)	7.9	(5.1)
$[N_\alpha,\!N_\pi,\!CO^-][N_\alpha,\!N_\pi]gtgg$	12.8	(15.6)	0.7	(2.2)	9.7	(12.5)	0.0	(0.0)
$[N_\alpha,\!N_\pi,\!CO^-][N_\alpha,\!N_\pi]gtgt$	14.4	(12.6)	9.0	(5.4)	11.6	(9.8)	11.1	(6.5)
$[N_\alpha,\!N_\pi,\!CO^-][N_\alpha,\!N_\pi,\!CO]$	22.5	(22.8)	8.8	(7.7)	18.1	(18.4)	5.5	(3.1)
$[N_{\alpha},\!N_{\pi},\!CO^{-}][CO_{2}^{-}](N_{\alpha}H^{+})$	21.2	(20.7)	18.1	(20.8)	19.1	(18.7)	20.6	(17.4)
$[N_\alpha, N_\pi, CO^-][N_\alpha, CO^-](N_\pi H^+)$	22.7	(24.4)	11.2	(13.4)	19.0	(20.7)	20.1	(19.1)
$[N_\pi, CO_2^-][N_\alpha, N_\pi]$	26.4	(26.7)	19.3	(18.8)	27.2	(27.5)	17.4	(14.9)
$[N_\alpha,\!CO^-][N_\alpha,\!N_\pi]ttgt$	44.9	(37.4)	56.0	(46.4)	45.1	(37.6)	63.6	(53.4)
$[\mathrm{CO_2}^-][\mathrm{N}_\alpha,\mathrm{N}_\pi,\!\mathrm{CO}]$	47.7	(45.9)	53.5	(50.2)	48.0	(46.2)	54.5	(49.9)
$[CO_2^-][N_\alpha,\!N_\pi]$	53.0	(50.7)	60.0	(56.6)	54.1	(51.8)	62.3	(57.2)
$[N_\alpha,\!CO^-][N_\alpha,\!N_\pi]tttt$	51.2	(44.0)	62.3	(53.2)	51.4	(44.2)	70.2	(60.3)
$[N_\alpha,CO^-][N_\alpha,N_\pi]gtgt$	67.0	(64.3)	63.2	(59.8)	65.9	(63.2)	71.7	(66.2)
$[N_\alpha,CO^-][N_\alpha,N_\pi]tcgt$	79.2	(72.2)	89.6	(80.3)	79.2	(72.2)	98.4	(88.7)
$[N_\alpha,CO^-][N_\alpha,N_\pi]gcgt$	98.6	(96.0)	93.8	(90.6)	97.1	(94.6)	103.3	(98.0)
$[N_{\alpha},\!CO^{-}][N_{\alpha},\!N_{\pi}]tcgt_{+}$	97.4	(91.0)	107.2	(99.3)	97.5	(91.1)	117.2	(108.0)

^a Relative single point enthalpies at 0 K and 298 K Gibbs energies (in parentheses) calculated at the level of theory specified using a 6-311+G(2d,2p) basis set and B3LYP/6-311+G(d,p) geometries and frequencies for ZPE and thermal corrections. ^b B3LYP-GD3BJ/6-311+G(2d,2p) energies using B3LYP-GD3BJ/6-311+G(d,p) geometries and frequencies for ZPE and thermal corrections.

Table 2. Metal-Ligand Bond Distances (Å) for M(His-H)(His)⁺ Complexes^a

_		(His-H)		His			
Structure	M-N _a ^b	M - N_{π}	М-О	$M-N_{\alpha}^{b}$	M - N_{π}	М-О	
$Zn^{2+}[N_{\alpha},N_{\pi},CO^{-}][CO_{2}^{-}](N_{\pi}H^{+})$	2.138	2.031	2.038	2.489 ^c		1.958	
$Zn^{2+}[N_\alpha,\!N_\pi,\!CO^{\scriptscriptstyle -}][N_\alpha,\!N_\pi]gtgg$	2.152	2.099	2.039	2.305	2.065		
$Zn^{2^+} [N_\alpha,\!N_\pi,\!CO^-][N_\alpha,\!N_\pi] gtgt$	2.215	2.089	2.012	2.235	2.074		
$Zn^{2+}\left[N_{\alpha},\!N_{\pi},\!CO^{-}\right]\!\left[N_{\alpha},\!N_{\pi},\!CO\right]$	2.138	2.120	2.041	2.188	2.153	2.890	
$Zn^{2^+}[N_{\alpha},\!N_{\pi},\!CO^-][CO_2^-](N_{\alpha}H^+)$	2.113	2.030	1.974	3.016 ^c		1.949	
$Zn^{2^+}[N_\alpha,\!N_\pi,\!CO^-][N_\alpha,\!CO^-](N_\pi H^+)$	2.209	2.085	2.039	2.204		2.006	
$Zn^{2^+}[N_\pi,CO_2^-][N_\alpha,N_\pi]$	2.878^{c}	2.058	1.941	2.129	2.030		
$Zn^{2+} \big[N_\alpha,\!CO^-\big] \big[N_\alpha,\!N_\pi\big] ttgt$	2.055		1.926	2.117	2.020		
$Zn^{2+}[\mathrm{CO_2}^-][\mathrm{N}_\alpha,\mathrm{N}_\pi,\mathrm{CO}]$	2.109 ^c		2.018	2.132	2.029	2.346	
$Zn^{2+}\left[CO_2^-\right]\!\left[N_\alpha,\!N_\pi\right]$	2.052^{c}		2.051	2.082	1.985		
$Zn^{2^+}[N_\alpha,CO^-][N_\alpha,N_\pi]tttt$	2.053		1.930	2.123	2.017		
$Zn^{2^+}[N_\alpha,\!CO^-][N_\alpha,\!N_\pi]gtgt$	2.103		1.917	2.117	2.009		
$Zn^{2+}[N_{\alpha},CO^{-}][N_{\alpha},N_{\pi}]tcgt_$	2.055		1.923	2.117	2.025		
$Zn^{2+}[N_\alpha,CO^-][N_\alpha,N_\pi]gcgt$	2.101		1.916	2.117	2.011		
$Zn^{2^+} \big[N_\alpha,CO^-\big] \big[N_\alpha,N_\pi\big] tcgt_+$	2.045		1.937	2.170	1.998		
$Cd^{2^{+}}[N_{\alpha},\!N_{\pi},\!CO^{-}][CO_{2}^{-}](N_{\pi}H^{+})$	2.364	2.265	2.295	2.436 ^c		2.208	
$Cd^{2^{+}}\left[N_{\alpha},\!N_{\pi},\!CO^{-}\right]\!\left[N_{\alpha},\!N_{\pi}\right]\!gtgg$	2.368	2.970	2.227	2.464	2.284		
$Cd^{2^+}\left[N_\alpha,\!N_\pi,\!CO^-\right]\!\left[N_\alpha,\!N_\pi,\!CO\right]$	2.346	2.351	2.216	2.416	2.336	2.767	
$Cd^{2^+}\left[N_\alpha,\!N_\pi,\!CO^-\right]\!\left[N_\alpha,\!N_\pi\right]\!gtgt$	2.379	2.300	2.216	2.435	2.269		
$Cd^{2^+}\left[N_\pi,\!CO_2^-\right]\!\left[N_\alpha,\!N_\pi,\!CO\right]$	2.499 ^c	2.305	2.238	2.404	2.275	2.828	
$Cd^{2^+}\left[N_\alpha,\!N_\pi,\!CO^-\right]\!\left[N_\alpha,\!CO^-\right]\!\left(N_\pi H^+\right)$	2.373	2.299	2.286	2.407		2.195	
$Cd^{2+}\left[N_{\pi},CO^{-}\right]\!\left[N_{\alpha},N_{\pi},CO\right]$	2.884 ^c	2.354	2.137	2.404	2.270	2.703	
$Cd^{2^{+}}\left[N_{\alpha},\!N_{\pi},\!CO^{-}\right]\!\left[N_{\alpha},\!N_{\pi}\right]\!gcgt$	2.383	2.283	2.240	2.448	2.260		
$Cd^{2+}\left[N_{\pi}\;,CO^{-}\right]\!\left[N_{\alpha},\!N_{\pi}\right]$	2.736 ^c	2.301	2.160	2.380	2.229		
$Cd^{2^+}\left[N_\pi \; ,\! CO_2^-\right]\! \left[N_\alpha,\! N_\pi\right]$	2.327 ^c	2.336	2.305	2.399	2.242		
$Cd^{2^+}\left[CO_2^-\right]\!\left[N_\alpha,\!N_\pi\right]$	2.248 ^c		2.244	2.330	2.199		
Cd^{2+} [N _{α} , N _{π} , CO^{-}][N _{π} , CO_{2}^{-}](N _{α} H ⁺) ^a Geometries are calculated at the B3LYI	2.386 P/ 6-311+G	2.269 (d.p) and B	2.197 3LYP/ def2	3.076 ^c	2.531 the zinc and	2.286	

^a Geometries are calculated at the B3LYP/ 6-311+G(d,p) and B3LYP/ def2-TZVP for the zinc and cadmium complexes, respectively. Distances between the metal center and heteroatoms further than 3.1 Å were omitted for clarity. ^b Except as noted. ^cM-O.

Table 3. Relative Enthalpies (0 K) and Gibbs Energies (298 K) of Cd(His-H)(His)⁺ Complexes in kJ/mol^a

Structure	B3LYP		B3LYP-GD3BJ ^b		B3P86		MP2(full)	
$[N_{\alpha},N_{\pi},CO^{-}][CO_{2}^{-}](N_{\pi}H^{+})$	0.0	(0.0)	1.5	(3.7)	0.0	(0.0)	8.4	(10.1)
$[N_\alpha, N_\pi, CO^-][N_\alpha, N_\pi]gtgg$	10.3	(8.5)	0.0	(0.0)	9.4	(7.6)	0.0	(0.0)
$[N_\alpha,\!N_\pi,\!CO^-][N_\alpha,\!N_\pi,\!CO]$	17.3	(15.1)	7.1	(5.6)	15.1	(12.9)	5.0	(4.6)
$[N_\alpha,\!N_\pi,\!CO^-][N_\alpha,\!N_\pi]gtgt$	16.4	(11.3)	15.4	(10.8)	15.8	(10.7)	16.2	(12.8)
$[N_\pi,CO_2^-][N_\alpha,N_\pi,CO]$	26.5	(24.6)	23.7	(23.9)	25.7	(23.8)	16.9	(16.8)
$[N_\alpha,\!N_\pi,\!CO^-][N_\alpha,\!CO^-](N_\pi H^+)$	27.8	(28.7)	16.4	(18.3)	25.6	(26.5)	26.3	(28.9)
$[N_\pi,CO^-][N_\alpha,N_\pi,CO]$	31.5	(26.7)	25.8	(23.3)	30.8	(26.0)	21.8	(18.7)
$[N_\alpha, N_\pi, CO^-][N_\alpha, N_\pi]gcgt$	42.9	(43.5)	31.6	(33.4)	38.2	(38.8)	30.5	(32.8)
$[N_\pi,CO^-][N_\alpha,N_\pi]$	39.0	(31.8)	37.5	(33.7)	39.3	(32.0)	31.6	(26.0)
$[N_\pi, CO_2^-][N_\alpha, N_\pi]$	48.2	(40.2)	53.1	(47.3)	48.6	(40.6)	45.4	(39.1)
$[\mathrm{CO_2}^-][\mathrm{N}_\alpha,\!\mathrm{N}_\pi]$	48.7	(44.0)	56.2	(52.2)	50.2	(45.5)	54.9	(51.9)
$[N_{\alpha},\!N_{\pi},\!CO^{\scriptscriptstyle{-}}][N_{\pi},CO_{2}^{\scriptscriptstyle{-}}](N_{\alpha}H^{\scriptscriptstyle{+}})$	61.1	(59.6)	53.1	(52.8)	56.9	(55.4)	51.5	(51.7)

^a Relative single point enthalpies at 0 K and 298 K Gibbs energies (in parentheses) calculated at the level of theory indicated using a def2-TZVPP basis set and B3LYP/ def2-TZVP geometries and frequencies for ZPE and thermal corrections. ^bB3LYP-GD3BJ/ def2-TZVPP energies using B3LYP-GD3BJ/ def2-TZVP geometries and frequencies for ZPE and thermal corrections.

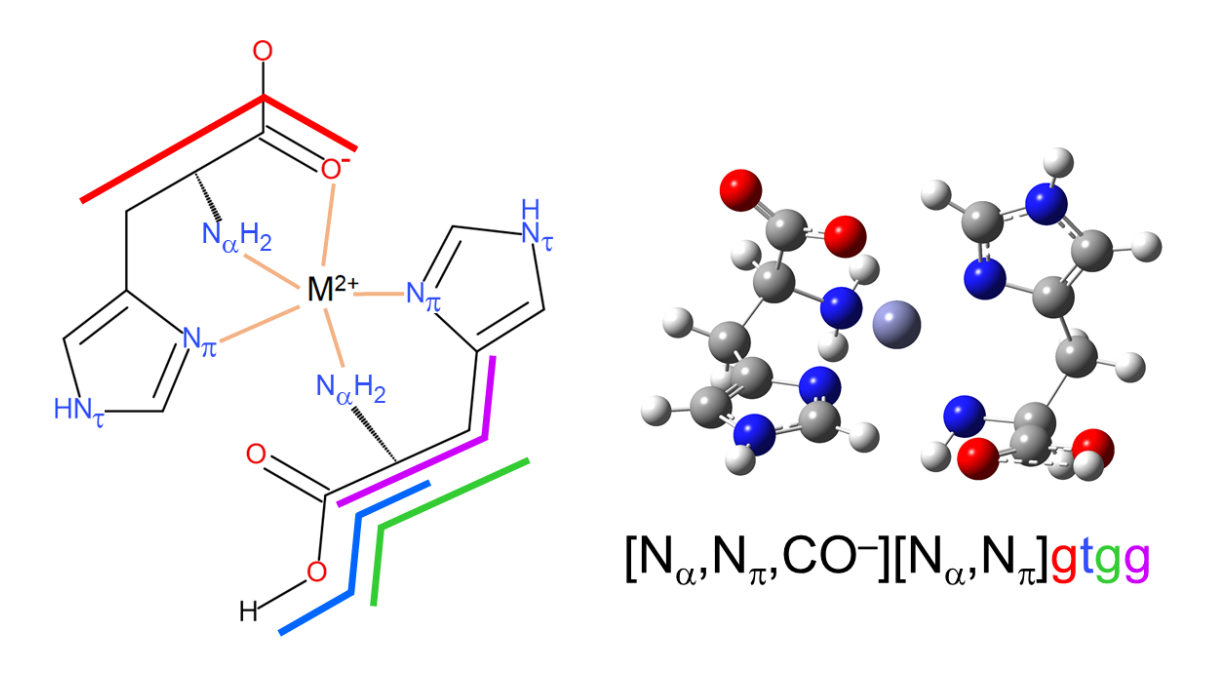


Figure 1. Illustration of the nomenclature used to describe conformers using the $Zn^{2+}[N_{\alpha},N_{\pi},CO^{-}][N_{\alpha},N_{\pi}]$ gtgg isomer for comparison. The orange lines indicate the metal coordination sites (in square brackets), while the red, blue, green, and purple lines correspond to the dihedral angles that are specified. (Red— \angle OCCC of (His-H) $^{-}$ ligand, blue— \angle HOCC, green — \angle OCCC, purple— \angle CCCC).

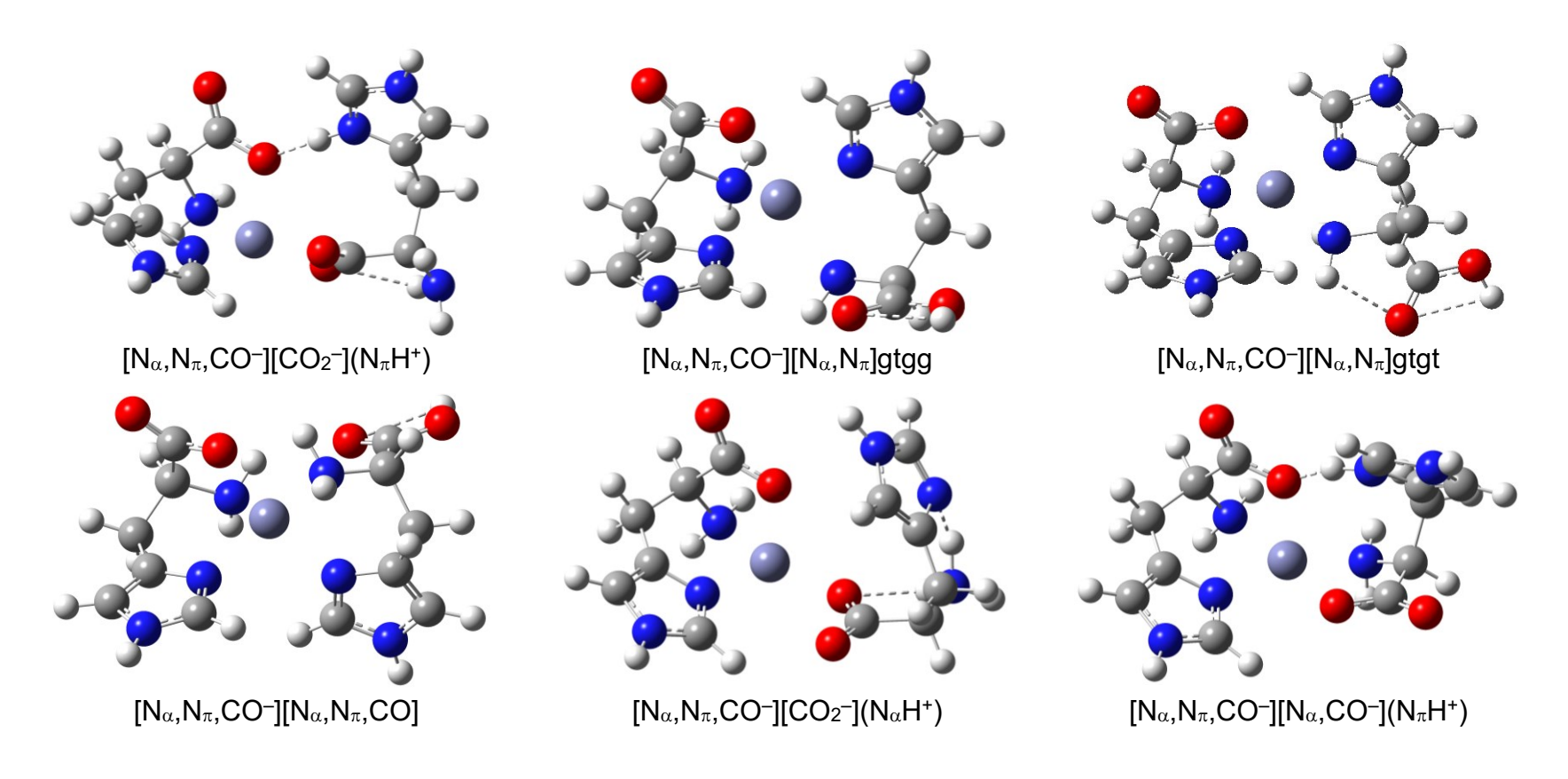


Figure 2. Structures of select Zn(His-H)(His)⁺ conformers calculated at the B3LYP/6-311+G(d,p) level of theory. Dashed lines indicate hydrogen bonds. (Red—oxygen, grey—carbon, white—hydrogen, blue—nitrogen, steel grey—zinc).

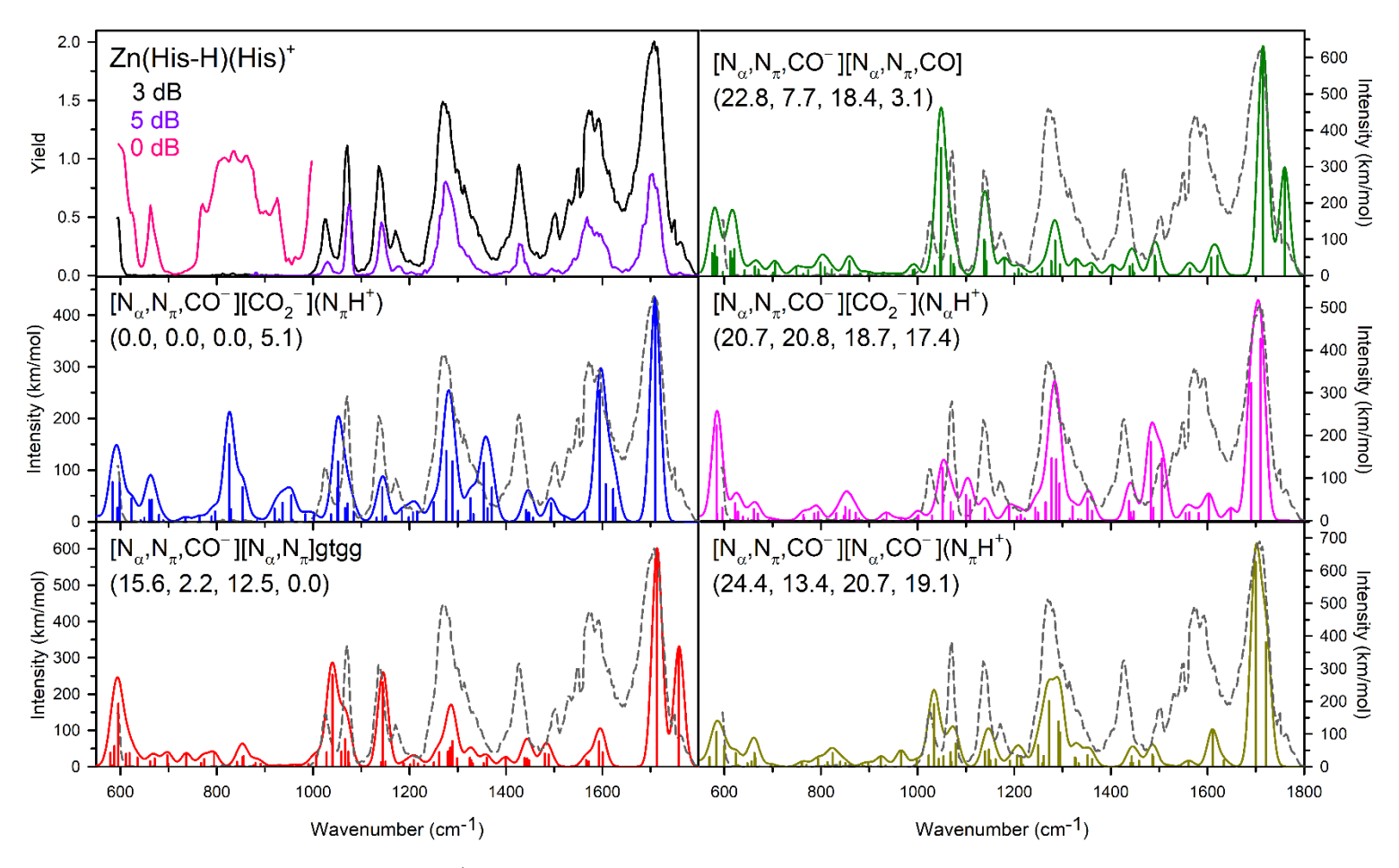


Figure 3. Comparison of the Zn(His-H)(His)⁺ experimental IRMPD action spectrum (black and grey dashed lines) with IR spectra calculated at the B3LYP/6-311+G(d,p) level of theory for low-lying conformers (in color). Relative 298 K Gibbs energies (kJ/mol) are given at the B3LYP, B3LYP-GD3BJ, B3P86, and MP2 levels, respectively, using the 6-311+G(2d,2p) basis set. Spectra taken with attenuated laser power or with additional laser pulses are indicated in color in the first panel. The 0 dB spectrum was taken with four FEL pulses instead of two.

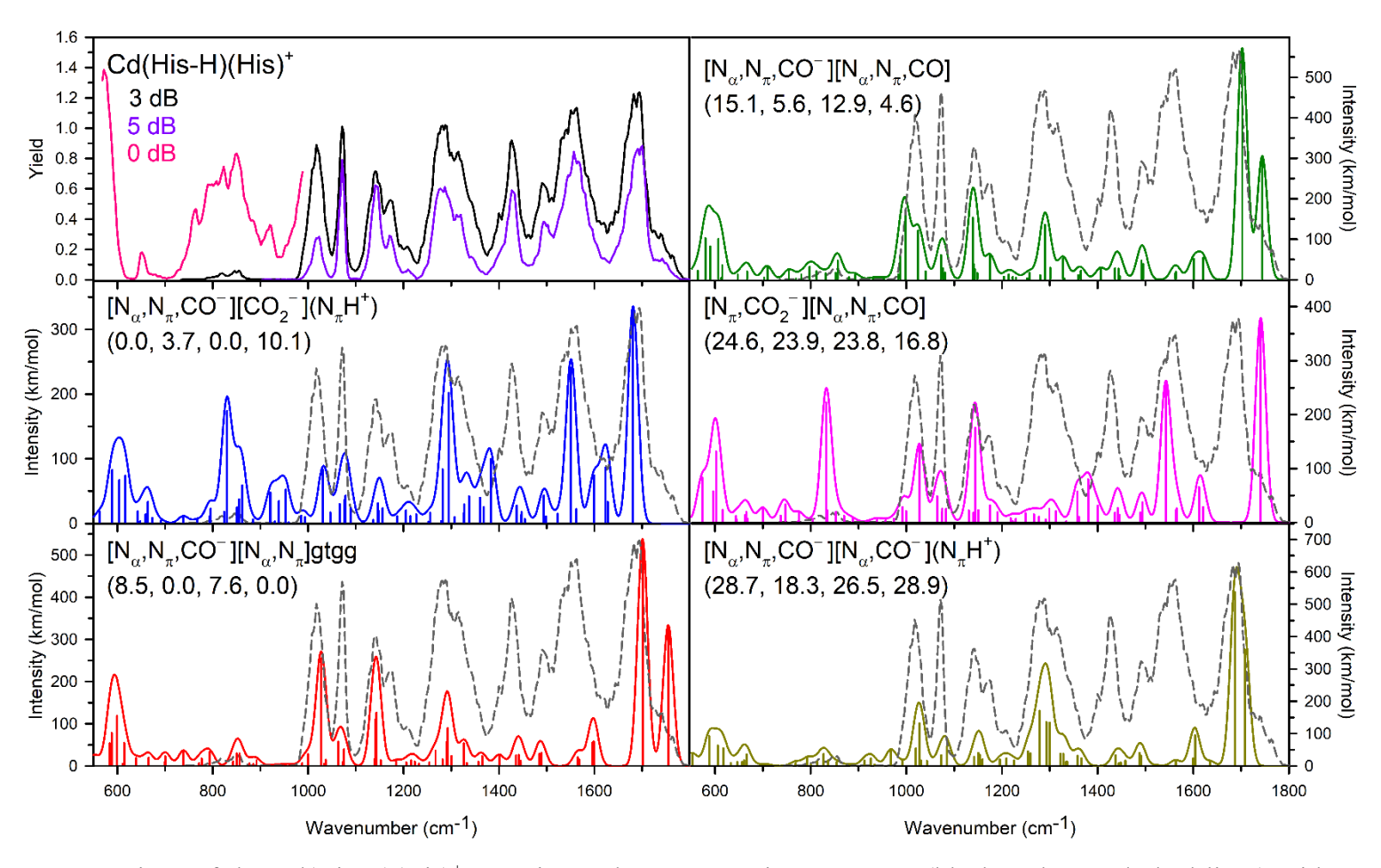


Figure 4. Comparison of the Cd(His-H)(His)⁺ experimental IRMPD action spectrum (black and grey dashed lines) with IR spectra calculated at the B3LYP/def2-TZVP level of theory for low-lying conformers (in color). Relative 298 K Gibbs energies (kJ/mol) are given at the B3LYP, B3LYP-GD3BJ, B3P86, and MP2 levels, respectively, using the def2-TZVPP basis set. Spectra taken with attenuated laser power are indicated by color in the first panel.

TOC graphic

